CHARGING AND DETECTION OF MESOSPHERIC DUST WITH INSTRUMENT SPID ON G-CHASER ROCKET

Tinna Gunnarsdottir[1], Henriette Trollvik[1], Ingrid Mann[1], Sveinung Olsen[1], Yngve Eilertsen[1], Tarjei Antonsen[1], Ove Havnes[1], Arne Bjørk[2], Erlend Restad[2], Åshild Fredriksen[1], Christoffer Boothby[2], Rikke Hansen [1], and Markus Floer[1]

[1]*Department of Physics and Technology, Tromsø, UiT The Arctic University of Norway, 9019 Tromsø, Norway. Email: tinna.gunnarsdottir@uit.no*

[2]*Faculty of Engineering Science and Technology, Narvik, UiT The Arctic University of Norway, Narvik, Norway*

ABSTRACT

The Smoke Particle Impact Detector (SPID) was flown on the G-Chaser student rocket that was launched from Andøya on 13 January 2019. SPID is a Faraday cup instrument with applied bias voltages to deflect the ambient plasma and a target area inside the probe designed to measure the dust particles by charge detection. The charging process of the dust particles in the detector is important for interpretation of the measurements and the influence of the charging models is discussed. Preliminary analysis of the SPID observations shows that ambient plasma and sunlight had an influence on the signals; further analysis is needed to retrieve information on impacting dust from the data.

Key words: SPID; G-Chaser; MSP; dust; nanoparticles; EISCAT.

1. INTRODUCTION

The Arctic University of Norway (UiT) designed an instrument called Smoke Particle Impact Detector (SPID) to measure small dust particles in the mesosphere. These dust particles, often called Meteoric Smoke Particles (MSPs), are thought to be nanometer sized particles that reside in the Earth's atmosphere at altitudes of around 50 - 100 km. They form from ablated meteoroid material, of which several tons enter Earths atmosphere each day [2]. MSPs are thought to play a role in mesospheric phenomena like Noctilucent Clouds (NLC), Polar Mesospheric Summer Echoes (PMSE) and possibly also Polar Mesospheric Winter Echoes (PMWE) [7]. They influence the mesospheric charge balance [3] as well as stratospheric clouds and weather in the lower layers of the atmosphere [4]. It is important to study these particles and gain more information on their composition, size and charge, because they are a part in various atmospheric processes. The small sizes and high altitude of the smoke particles make it difficult to study them with remote sensing. Little information has been gained by radar and lidar. Satellite observations mainly provide information on the smoke particles when encased in ice in the cold summer mesosphere at high and mid latitudes [9]. Rockets are however a good method to study the smoke particles since they provide the opportunity for in-situ measurements. SPID was developed by UiT with heritage from the rocket probes DUSTY and MUltiple Dust Detector (MUDD), also designed and built by UiT. These probes were previously designed to measure the smoke particles in the cold mesosphere during the summer when the particles are encased in ice. SPID was launched successfully for the first time on the top-deck of the G-Chaser student rocket on 13th of January 2019 at 09:13 UTC from Andøya Norway. Here an overview of the probe and its measurements is given; first some information on the G-Chaser program is introduced and then an overview of the SPID probe is given. The probes design and the way it detects smoke particles is discussed and the currents measured by SPID from the rocket launch are examined.

2. G-CHASER

The G-Chaser student rocket was a part of the Grand Challenge Initiative Cusp project; a collaboration between Colorado Space Grant Consortium, NASA Wallops Flight Facility, Andøya Space Center and University of Oslo. This was the only student rocket in the program and it contained instruments from seven universities from Norway, USA and Japan. The rocket launch was also a part of the RockSat-XN program, which is designed to allow students at a university level to design and launch an experiment on a rocket. The rocket type used for the G-Chaser launch was a Terrier Improved Malemute, a two stage rocket designed by NASA [17]. Fig. 1 shows a sketch of the payload-section of the rocket, with the initials of each university marking the placement of their respective instrument. The top deck is shown on the right with UiT marking the place for the SPID instrument; sharing the nose-cone section with the instrument PARM that was designed by JAXA and Nagoya

University. Other instrument teams participating in the rocket launch were Andøya Space Center with University of Oslo (UiO), Capitol Technology University (CTU), Pennsylvania State University (PSU), University of New Hampshire (UNH) and University Of Puerto Rico (UPR).

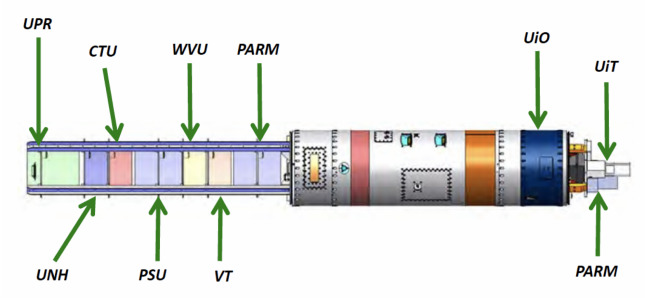

Figure 1. Payload section of G-Chaser student rocket, showing the designated sections for each University/team. UIT/SPID is situated in the nosecone section along with Japanese instrument PARM. Figure: NASA Wallops Flight Facility

3. SMOKE PARTICLE IMPACT DETECTOR

The Smoke Particle Impact Detector is an impact probe and a Faraday cup, designed to measure free nanometer-sized smoke particles in the warm winter mesosphere. The general design with its dimensions is given in Fig. 2. The probe is a hollow cylinder with 50 mm long openings in the bottom situated on top of the electronics box. It has a total length of 251 mm as can be seen in the bottom part of the figure. A top view of the probe can be seen in the upper part of the figure, showing the 82 mm in diameter probe on top of the 70x70 mm electronics box. Inside the cylinder (60 mm in diameter) is an inclined stainless steel plate to measure incoming particles with the middle plate. Two silver coated brass grids are located on either side of the cylinder openings to shield out ambient plasma from entering the probe. Their respective order and the bias potentials applied to them are given in Tab. 1. Applying the bias voltage to the grids shields out the ambient plasma. The middle plate is also biased to facilitate the movement of negatively charged particles away from the plate hence increasing the detection probability. A vertical cross-section of the middle plate is shown in Fig. 3. The middle plate is made up of 7 concentric rings of stainless steel. The rings are all inclined towards the centre in the bottom, with 70° to the normal. This inclination leads to maximum charge generation by the incoming particles and thus a maximum probability of small particle detection [8, 14]. SPID shares the nose-cone section with the instrument PARM as can be seen in Fig. 4, the image is taken at the final integration of the rocket at Andøya Space Center. Because SPID is designed to measure particles smaller than 2 nm, the geometry was modified in comparison to the previous instruments to allow airflow through the probe and reduce the shock front. Airflow simulations were initially done to test the geometry design as well as to determine if sharing the nose-cone might affect the airflow through SPID, with results discussed in detail elsewhere [15, 16].

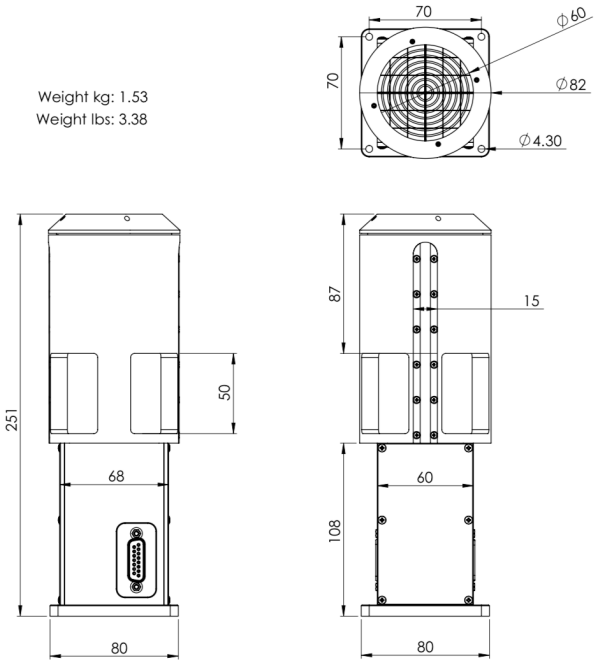

Figure 2. The SPID probe shown with its respective dimensions in millimeters. Top right shows the top view where the grids and middle plate can be seen inside. Bottom left and right show two lateral views of the cylinder-shaped probe on top of the electronics box.

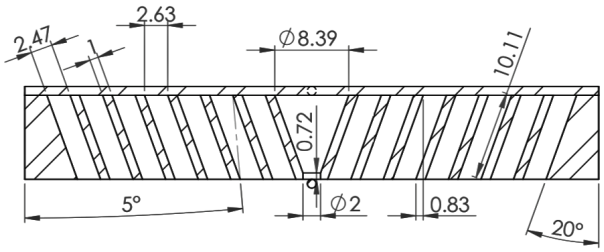

Figure 3. Vertical cross-section of the middle plate inside SPID, its dimensions given in millimeters.

Table 1. Composition and bias potential settings off the grids and middle plate inside the SPID probe. In order of closest to the top to the closest to the bottom.

Part	Material	Potential
Grid Top 1	Brass coated with silver	$+10V$
Grid Top 2	Brass coated with silver	$-10V$
Middle Plate	AISI 316L Stainless Steel	$-2V$
Grid Bottom 2	Brass coated with silver	$+10V$
Grid Bottom 1	Brass coated with silver	$-10V$

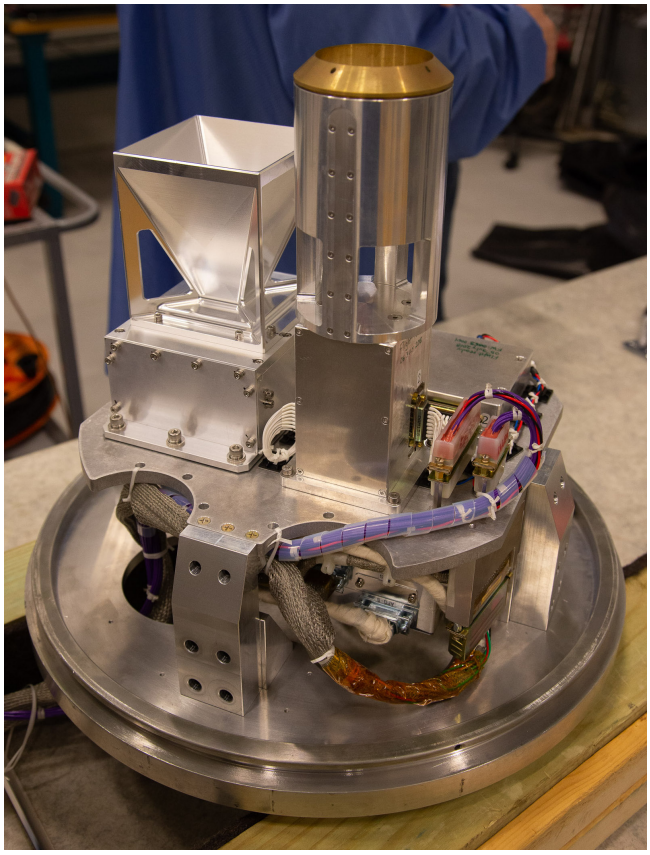

Figure 4. Nosecone section of G-Chaser rocket prior to assembly at Andøya Space Center. SPID probe is shown on the right along with instrument PARM on the left. Figure: NASA/Wallops Flight Facility

4. CHARGE DETECTION

Dust particles that enter the probe, whether previously charged or neutral, will collide with the slanted middle plate and generate charge. The current that we measure is a result from the particles colliding or sliding on the plate as well as any initial charge the particles might have. As the particles come into contact with the plate a charge can be transferred between them. The generated charge can be either positive or negative, all depending on the difference in work function between the particles and plate material. The work function of a material is the energy needed to eject an electron from its surface [6, 12]. The middle plate is made of stainless steel with a work function around 4.3-4.4 eV [10]. The composition of the dust is not exactly known, which induces an uncertainty in describing the interaction. A possible work function value for MSPs of 4.0 - 4.6 eV is discussed by Rapp et al. [13], which would be very close to the stainless steel work function value. To accurately describe the charge exchange many factors need to be considered; the incoming velocity of the particles, the minimum distance between them, the composition of the plate and particles as well as the plates surface roughness. First by considering the interaction as a close contact between two capacitors the total charge Q_c that is transferred in the collision is given by Eq. 1 [12]:

$$Q_c = C_0 \, V_c \tag{1}$$

Where C_0 is the capacitance between them at a certain separation distance and V_c is the contact potential difference of the particle against the plate given by Eq. 2 [6, 12]:

$$V_c = -\frac{\phi_p - \phi_s}{e} \tag{2}$$

With ϕ_p and ϕ_s denoting the work function of the particle and the plate respectively and e denoting the elementary charge. How the capacitance between the plate and the particle is described depends on the charging model chosen. A comparison of several possible charging models [1, 11, 12, 18] is given in Gunnarsdottir [5], and these show that the estimated charge production has a large variation depending on the model used. The most promising model in this instance is that of Wang and John [18] because it accounts for particle deformation at impact due to the large speed of the particles hitting the plate. The charging generated by the model from Wang and John [18] is given in Eq. 3:

$$Q_c = \pi r \, \alpha_m \epsilon_0 \frac{V_c}{Z} \tag{3}$$

Here V_c is the contact potential mentioned above, Z is the separation between the particles and the plate (very small in the case of nano particles), r is the particle radius and α_m is a variable defined by material properties and is further explained in Appendix A. Now any model chosen to represent the generated charge by incoming particles would have to be tested against size and altitude distribution models of dust. Testing the middle plate of SPID would also be beneficial in order to better understand the interaction of dust with the plate and its overall efficiency.

An ideal scenario would be to test the probe in a laboratory setting with nanometer sized high velocity particles impacting on it to accurately test the probes charge generation characteristics, but in practice this is extremely hard to accomplish. Some additional factors would also be beneficial to study further for example the surface properties of the middle plate, its roughness and surface impurities and contamination like oxidation layers among others. This complicates the data analysis since it requires several assumptions on the incoming particles as well as on the interaction of the dust with the plate. Testing the SPID probe with middle plates of different material with different work functions would also be beneficial in order to gain more knowledge on the composition of MSPs. The effect that the bias of -2V on the middle plate has on the charge transfer also remains to be tested to see how the energy levels of the plate and the dust are altered when they come into contact.

5. MEASUREMENTS AND RESULTS

SPID measured a current on the middle plate as well as at the four silver grids during the entire rocket flight. Unfortunately the two top grids went into saturation at the opening of the nose-cone and thus they give no information on the shielding of the plasma or what was entering the probe. The current measured by the middle plate and the two bottom grids can be seen in Fig. 5, where the top figure shows the current measured on the middle plate from right before the nose-cone is opened. The middle figure shows the current measured on the GB2 grid which has a potential of +10 V and thus will primarily measure negative particles, and the bottom figure shows the GB1 grid with a potential setting of -10 V and thus measures mainly positive particles. Initial examination of these measurements suggest that they were affected by positive ions entering the probe as well as sunlight hitting the grids. This also contributed to an increase in the amplitude of the coning motion seen in the recorded currents. This coning motion is mainly visible in the middle plate currents and the GB2 current. To what degree these contributions dominate the signal will be a topic for future study. Several interesting areas of the signals will need to be examined in detail and some of these are discussed by Trollvik [15, 16]. During the launch the EISCAT radars, both VHF (224 MHz) and UHF (931 MHz), were operating for the entire flight and we could compare the possible ion density contribution to the measured current. The UHF was pointing at the location of the launch while the VHF was pointing straight up. Due to data quality the VHF measurements were used for the initial data comparison [5]. The current contribution from incoming ions can be calculated by Eq. 4:

$$I_i = Ae\ \alpha\ v_{rocket} N_i \tag{4}$$

Where N_i is the ion density estimated from the EISCAT measurements, α is the collection efficiency, e is unit charge, v_{rocket} is the rocket velocity and A is the area of the SPID opening. The estimated ion current is shown in Fig. 6 where collection efficiency α was taken from Trollvik [16]. The plate and grids are influenced by photoemission caused by sunlight, where sunlight ejects electrons from the material that is illuminated. The contribution from the induced photocurrent on the probe grids was estimated by considering the light path and attenuation in the atmosphere in a similar way as was done by Giono et al. [4]. This gives the amount of photons at a given rocket altitude, further taking into account the material properties and the spin of the rocket the photocurrent can be estimated. A more thorough analysis could include ray tracing calculations to accurately determine the amount of time the grids are being exposed to the sun to estimate more accurately the amount of solar contribution. As well as testing the photo-emitting and reflecting properties of the grid would help to get a more accurate contribution to the measured currents. The photocurrent contribution Q_{ph} can be calculated by Eq. 6 [5]:

$$Q_{ph}(h, \lambda) = N_{ph}(h, \lambda)\ \sigma(h, \lambda)\ \beta \tag{5}$$

Here N_{ph} is the number of photons generated at each altitude segment h for different wavelengths λ of incident sunlight, σ is the optical depth per altitude and wavelength, and β is the fraction of a rotation period that the rocket is illuminated. More details in [4, 5].

At the time of the launch the sun was below the horizon by about 5° and so the rocket is in sunlight from about 25 km altitude and upwards. However due to atmospheric attenuation the sun does not have as much affect until above 70-80 km mainly due to ozone absorption and the atmospheric path the sun-rays have to cross in this particular instance [5]. From 80 to 100 km the photoemission contribution gradually increases to around 0.4 mA total for the entire payload and stays around that number up to the apogee of 184 km. This seems to fit the general increase in current signal as can be shown in Fig. 6. Here, shown in blue, is the possible contribution from the ions (using electron density from EISCAT VHF measurements) and, shown in red, is the possible ion current along with a 2.5 % contribution from photoemission due to direct sunlight. So the contribution due to sunlight is around 1 to 2.5 % of the total photoemission current incident on the probe.

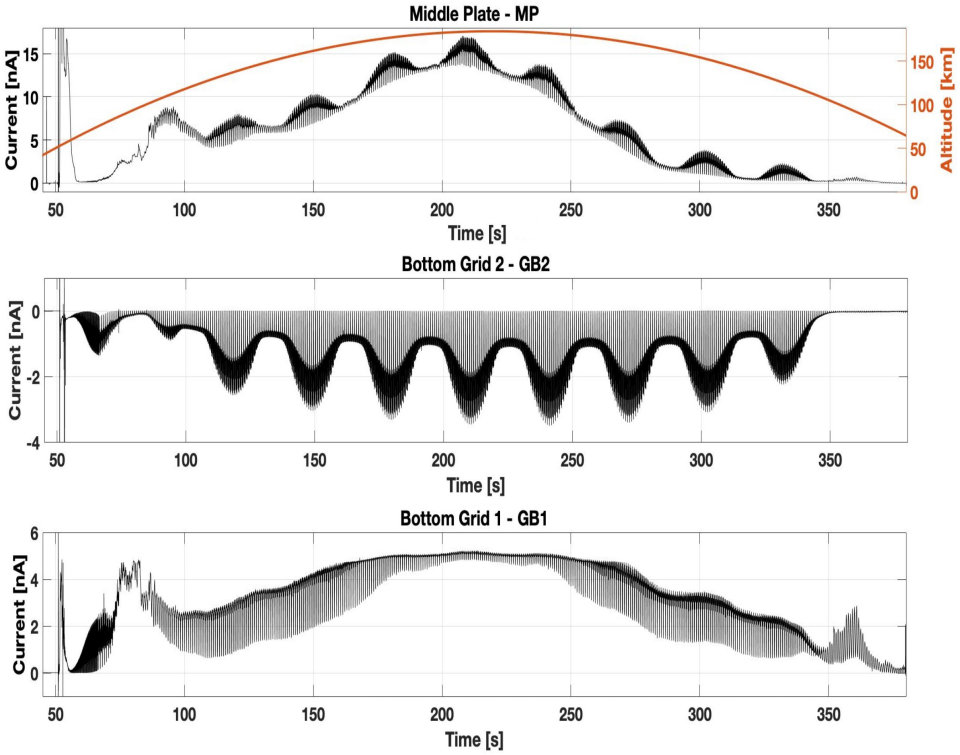

Figure 5. Current measured on the middle plate, the bottom grid 1 (GB1) and bottom grid 2 (GB2) during the rocket flight. The bias potentials are listed in Tab. 1. Also shown in the plot for the middle plate is the rocket altitude, in red.

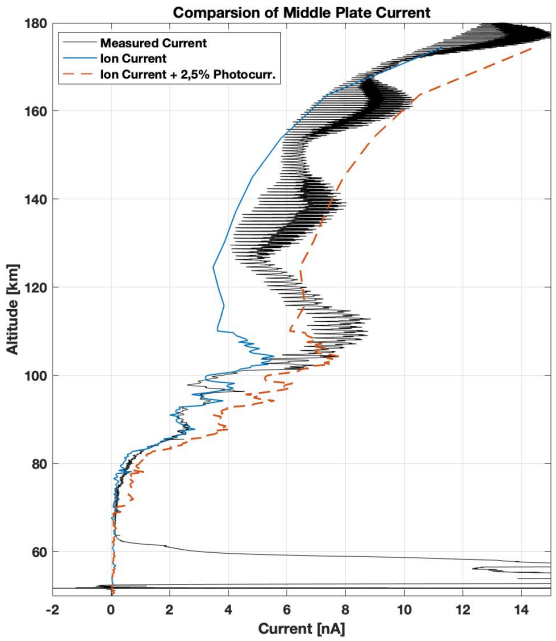

Figure 6. Current measurements from SPIDs middle plate shown in black compared to ion density current (using EISCAT measurements) in blue, in red is shown the ion density current combined with a 2.5 % current caused by photoemission due to plate being in direct sunlight.

The grid GB1 has a negative bias potential of -10 V and its signal is possibly influenced by ions. Fig. 7 shows the current measured at grid GB1 on the up-leg of the rocket path. Also shown is an ion current from EISCAT observations made during the flight. Here there is a larger discrepancy between the signal and the ion current due to the calculated ion current not accounting for lesser airflow into the probe as well as the smaller grid size. The area 100 to 110 km shows a larger difference than for the rest of the signal. Whether this is due to a larger concentration of positive ions at the rocket than what is measured by EISCAT will need to be studied further since the VHF radar was pointed upwards and not at the location of the rocket. Here the contribution from direct sunlight can be seen in the signal, however not as strongly as it is seen in Fig. 8 which shows the GB2 grid which has a positive bias of +10 V. The GB2 current shows a strong increase in current with altitude and a strong coning influence that is reinforced by direct sunlight on the grids. This can be seen in the low oscillating frequency due to coning and the other high frequency due to the spinning of the rocket. During each spin the current goes to zero when the grid is not in direct sunlight. An exception is the altitude range 60 - 80 km where influence of sunlight should be small because of the atmospheric absorption; yet the measured current is quite high, corresponding to a similar positive current as measured on the GB1 grid. Here the current also does not go to zero but has a small increase

corresponding to the signal peak in that altitude range. Indicating that the grid might be measuring negative particles, possibly dust particles coming into the probe or negatively charged particles coming from the middle plate or electrons entering due to the large airflow.

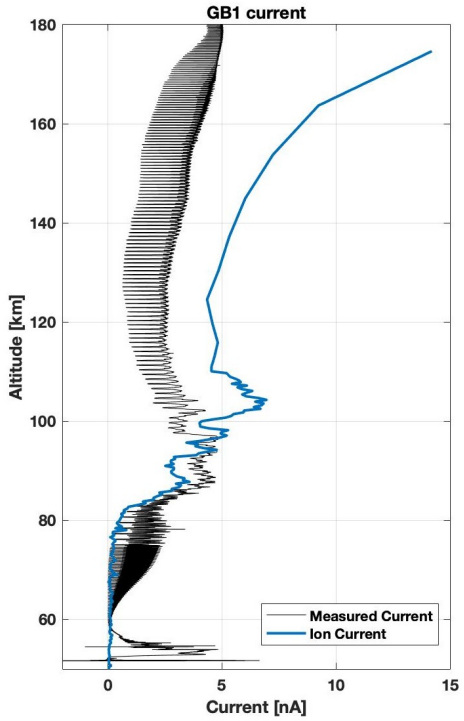

Figure 7. Current measured at GB1 shown along with an ion current estimated based on EISCAT observations, this current is not corrected for airflow and slower speed of the rocket.

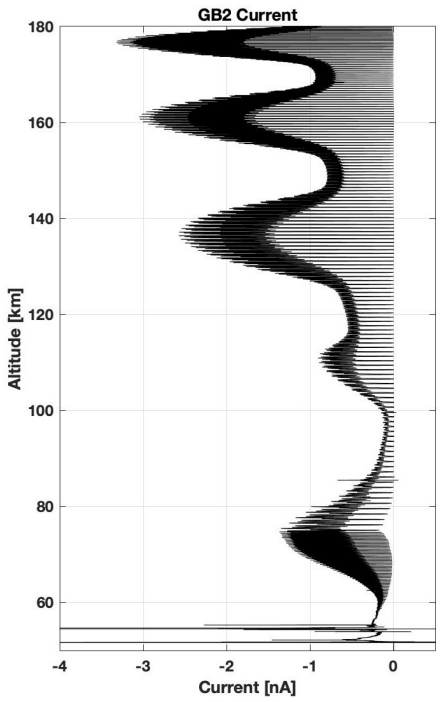

Figure 8. Current measured at GB2 on the up-leg of the rocket flight.

6. CONCLUSION

The SPID probe worked as it should, measuring currents on the middle plate and the two bottoms grids for the entire flight, however with two grids having saturated signal. Both the plate and the bottom grids are influenced by direct sunlight mainly from about 70-80 km altitude and upwards. We assume that the plasma shielding was ineffective and that ions entered the probe. Both he middle plate as well as the GB1 grid signals have a negative bias potential and thus mainly measure positive particles, presumably ions. This is supported by the estimated ion currents. To determine the possible contribution from dust on the middle plate signal we need to make assumptions on the dust charging. We discussed uncertainties in the charging models. Another difficulty lies in accurately determining the correct contribution from ions and sunlight which is needed to determine the total fraction of the signal that can be due to dust particles, initially charged or neutral, entering the probe. More thorough investigations and tests are needed in order to separate these; for example plasma chamber tests, airflow test, as well as other tests mentioned above. A new launch for SPID would be very beneficial to compare with this one, as well as launching a similar probe designed with further optimizing the airflow well as with different middle plate composition.

ACKNOWLEDGMENTS

Funding for the project was provided by The Norwegian Research Council, projects NFR 275503 and 240065, by UiT Rektors fund, Department of Physics and Technology and Faculty of Engineering and Technology. Student travel was funded by the Norwegian Space Agency.

This project was a team effort in collaboration between two campuses, Tromsø and Narvik, of the Arctic University of Norway. With Narvik handling the hardware and software side of the project and Tromsø handling the administration, simulations and dust model calculations as well as drawing, designing and building the probe. Professor Åshild Fredriksen was the team leader and project initiator that made this all happen. Along with faculty from Tromsø and Narvik were Sveinung Olsen, Yngve Eilertsen, Ingrid Mann, Tarjei Antonsen, Arne Bjork and Ove Havnes. Studens working on the project were Henriette Trollvik, Tinna Gunnarsdottir, Rikke Hansen and Markus Floer from campus Tromsø and Erlend Restad, Christofer Boothby, James Alexander Cowie, Vetle Tronstad and Christer Nordby from campus Narvik.

Electron density measurements during launch were used from EISCAT VHF radar. EISCAT is an international association supported by research organisations in China (CRIRP), Finland (SA), Japan (NIPR and ISEE), Norway (NFR), Sweden (VR), and the United Kingdom (UKRI).

APPENDIX A

The charge a particle can gain in a high velocity impact accounting for plastic deformation of the particle is given by Wang and John [18]:

$$Q_c = \pi r\ \alpha_m \epsilon_0 \frac{V_c}{Z} \tag{6}$$

Where r is the particle radius, ϵ_0 is the permittivity in free space, V_c is the contact potential difference given by equation 2 and α_m is a constant and is given by:

$$\alpha_m = 0.5\ b_2 + \sqrt{b_1^2 + b_2^2} \tag{7}$$

Where b_1 and b_2 are constants given by:

$$b_1 = v_y \sqrt{\frac{m}{P_y \pi r}} \tag{8}$$

$$b_2 = \frac{8\pi^2 r^2 P_y^2}{27\ C_k^2} \tag{9}$$

Here m is the particle mass, P_y is the yield pressure for the particles, which is the pressure the particles can handle before plastic deformation occurs. The constant C_k is given by

$$C_k = \frac{4\sqrt{r}}{3\pi\ (k_p + k_s)} \tag{10}$$

Where the mechanical constants k_p for the particle and k_s for the plate are defined by [12]:

$$k = \frac{1 - \upsilon^2}{\pi E} \tag{11}$$

Where υ is the Poisson's ratio and E is the young's modulus for each material. At the moment of maximum deformation the velocity v_y is given by:

$$v_y = v_0 \Big[1 - \frac{\pi^8 P_y^5 (k_p + k_s)^4}{40\ v_0^2\ \rho_p}\Big] \tag{12}$$

Where v_0 is the initial impact velocity and ρ_p is the particle density

REFERENCES

[1] Adams, N. and Smith, D. (1971). Studies of microparticle impact phenomena leading to the development of a highly sensitive micrometeoroid detector. *Planetary and Space Science*, 19(2):195–204.

[2] Antonsen, T., Havnes, O., and Mann, I. (2017). Estimates of the size distribution of meteoric smoke particles from rocket-borne impact probes. *Journal of Geophysical Research: Atmospheres*, 122(22).

[3] Baumann, C., Rapp, M., Kero, A., and Enell, C.-F. (2013). Meteor smoke influences on the d-region charge balance–review of recent in situ measurements and one-dimensional model results. In *Annales Geophysicae*, volume 31, pages 2049–2062. Copernicus GmbH.

[4] Giono, G., Strelnikov, B., Asmus, H., Staszak, T., Ivchenko, N., and Lübken, F.-J. (2018). Photocurrent modelling and experimental confirmation for meteoric smoke particle detectors on board atmospheric sounding rockets. *Atmospheric Measurement Techniques*, 11(9):5299–5314.

[5] Gunnarsdottir, T. (2019). Charging effects and detection of mesospheric dust with the instrument spid on the g-chaser rocket. Master's thesis, UiT Norges arktiske universitet.

[6] Harper, W. (1951). The volta effect as a cause of static electrification. *Proceedings of the Royal Society of London. Series A. Mathematical and Physical Sciences*, 205(1080):83–103.

[7] Havnes, O., Gumbel, J., Antonsen, T., Hedin, J., and La Hoz, C. (2014). On the size distribution of collision fragments of nlc dust particles and their relevance to meteoric smoke particles. *Journal of Atmospheric and Solar-Terrestrial Physics*, 118:190–198.

[8] Havnes, O. and Næsheim, L. I. (2007). On the secondary charging effects and structure of mesospheric dust particles impacting on rocket probes.

[9] Hervig, M. E., Brooke, J. S., Feng, W., Bardeen, C. G., and Plane, J. (2017). Constraints on meteoric smoke composition and meteoric influx using sofie observations with models. *Journal of Geophysical Research: Atmospheres*, 122(24).

[10] Inc., A. A. S. M. (Accessed: 2019-04-01). Stainless Steel 316L: Material properties.

[11] John, W. (1995). Particle-surface interactions: charge transfer, energy loss, resuspension, and deagglomeration. *Aerosol science and technology*, 23(1):2–24.

[12] Matsusaka, S., Maruyama, H., Matsuyama, T., and Ghadiri, M. (2010). Triboelectric charging of powders: A review. *Chemical Engineering Science*, 65(22):5781–5807.

[13] Rapp, M., Plane, J., Strelnikov, B., Stober, G., Ernst, S., Hedin, J., Friedrich, M., and Hoppe, U.-P. (2012). In situ observations of meteor smoke particles (msp) during the geminids 2010: constraints on msp size, work function and composition. In *Annales geophysicae*, volume 30, pages 1661–1673. Copernicus GmbH.

[14] Tomsic, A. (2003). Collisions between water clusters and surfaces.

[15] Trollvik, H. M. T. (2019a). On the meteoric smoke particle detector spid: Measurements and analysis from the g-chaser rocket campaign. Master's thesis, UiT Norges arktiske universitet.

[16] Trollvik, H. M. T. (2019b). Simulations and observations by the meteoric smoke particle detector(spid) part of the g-chaser rocket campaign. *ESA PAC 2019 Proceedings*.

[17] Wallops Fligth Facility (2016). Rocksat-xn user's guide, grand challenge student rocket.

[18] Wang, H.-C. and John, W. (1988). Dynamic contact charge transfer considering plastic deformation. *Journal of aerosol science*, 19(4):399–411.